

POPDx: An Automated Framework for Patient Phenotyping across 392,246 Individuals in the UK Biobank Study

Lu Yang^{1*}, Sheng Wang⁴ and Russ B. Altman^{1,2,3*}

¹Department of Bioengineering, Stanford University, Stanford, CA 94305, USA,

²Department of Genetics, Stanford University, Stanford, CA 94305, USA,

³Department of Medicine, Stanford University, Stanford, CA 94305, USA

⁴Paul G. Allen Scholl of Computer Science and Engineering, University of Washington, Seattle, WA 98195, USA

*To whom correspondence should be addressed.

ABSTRACT

Objective

For the UK Biobank standardized phenotype codes are associated with patients who have been hospitalized but are missing for many patients who have been treated exclusively in an outpatient setting. We describe a method for phenotype recognition that imputes phenotype codes for all UK Biobank participants.

Materials and Methods

POPDx (Population-based Objective Phenotyping by Deep Extrapolation) is a bilinear machine learning framework for simultaneously estimating the probabilities of 1,538 phenotype codes. We extracted phenotypic and health-related information of 392,246 individuals from the UK Biobank for POPDx development and evaluation. A total of 12,803 ICD-10 diagnosis codes of the patients were converted to 1,538 Phecodes as gold standard labels. The POPDx framework was evaluated and compared to other available methods on automated multi-phenotype recognition.

Results

POPDx can predict phenotypes that are rare or even unobserved in training. We demonstrate substantial improvement of automated multi-phenotype recognition across 22 disease categories, and its application in identifying key epidemiological features associated with each phenotype.

Conclusions

POPDx helps provide well-defined cohorts for downstream studies. It is a general purpose method that can be applied to other biobanks with diverse but incomplete data.

INTRODUCTION

Artificial intelligence (AI) allows machines to recognize patterns in electronic patient records (medical notes, laboratory tests, medications, and diagnosis codes). With increasing amounts of data available, machine learning algorithms have enabled healthcare applications, ranging from the detection of pneumonia in frontal chest X-ray images to the identification of heart failures in clinical notes [1, 2]. There have also been growing efforts to predict clinical events, i.e., the automatic prediction of patient phenotypes with data-driven approaches [3, 4]. However, most studies have focused on a small number (<10) of disease diagnoses (e.g., assessing the risks for cardiovascular diseases), and so their general utility is limited [5]. Large-scale biobanks with genetic and phenotypic data are a vital source for studying a wide range of diseases. Cohort studies such as UK Biobank support broad multi-phenotype research with a range of data including biological samples, physical measures, questionnaires related to socio-demographic conditions, lifestyle and health-related factors, and electronic medical records [6, 7, 8]. Unfortunately, missing data is common. In the UK Biobank, many individuals who have been treated exclusively on an outpatient basis have missing phenotype labels. To maximize the utility of these data, large-scale patient phenotyping is necessary but expensive, time-consuming, and difficult. Currently, only a subset conditions have available algorithms for recognition of unlabeled phenotypes [9, 10, 11]. These algorithms require extensive task-defined preprocessing and ad-hoc feature engineering [7, 8, 11]. A disease recognition system that recognizes multiple phenotypes would be helpful in defining patient cohorts for downstream studies. Recognizing rare phenotypes with small (or non-existent) training data is a particular challenge, even in large biobanks.

Rare diseases affect about 3.5–5.9% of people worldwide [12]. While predictive models exist for common diseases using carefully curated datasets in sufficient volume to allow statistical

characterization, detecting rare or unseen diseases remains difficult [13, 14]. There is currently no framework that evaluates individual patients for rare and common diseases in parallel. Rare diseases can be associated with noisier data because of inconsistent diagnostic criteria and clinician uncertainty [15]. The phenotype-driven approaches to rare diseases therefore typically rely on difficult-to-assemble cohorts. For rare diseases, patient sample sizes follow a long-tailed class distribution. Conventional machine-learning methods typically perform better on the majority class and exhibit poor predictive accuracy on rare disease classes. In recent years, semi-supervised and supervised methods have helped improve performance on imbalanced datasets, e.g., single-cell annotations to classify cells into cell types and cell states absent or present in the training data [16, 17]. However, the techniques they employ have not been applied to multi-phenotype recognition with heterogeneous patient data. We developed POPDx to associate patients with phenotypes for both common and rare phenotypes. It combines embedded representations of disease features with NLP-based encoding of the text and network-based embedding of the Human Disease Ontology to regularize the disease feature representation. We train POPDx with numerical and categorical data including health records, laboratory tests, individual demographics, lifestyles, and environmental exposures. We compile clinical profiles of 392,246 patients in UK Biobank [6] and perform imbalanced learning with 1,538 disease and health-related labels. Our phenotype recognition algorithm outperforms the state-of-the-art predictive models. It recognizes a comprehensive set of phenotypes, and makes the following contributions:

1. It manages missingness, noise, and high dimensionality typical in EHR data.
2. It scales to population-scale sets of patients and phenotypes.

3. It leverages the Human Disease Ontology to derive an integrated model for 1,538 phenotypes, that can recognize phenotypes even when there are few or no examples of these phenotypes in the training set.

RESULTS

Overview of POPDx

Figure 1A summarizes POPDx. First, the raw data are downloaded from UK Biobank. Second, the collected data are transformed into 38,663 patient features and 1,538 associated phenotype codes. Third, we apply POPDx to recognize a diverse set of phenotypes, yielding a profile of phenotypes for each patient. Because the training data for many phenotypes is sparse, we introduce the use of ontological relationships to supplement the raw data. In particular, POPDx framework leverages disease ontological relationships (as represented in the Human Disease Ontology) embedded in a low-dimensional space and then projects the high-dimensional features of each patient to the same low-dimensional embedding space by a nonlinear transformation (Figure 1B and 1C). This has been used in other settings and has been shown to improve classification for classes with zero or few examples [16]. The framework encodes the patient data through a bilinear framework with two hidden layers of POPDx architecture and a matrix transformation (Figure 1B). The resulting outputs denote the probabilities of each phenotype for each patient. POPDx is written in Python and is made available as an open-source package. Importantly, with a pre-trained model, we can recognize 1,538 disease phenotypes given an input patient matrix in a few minutes on a GPU.

392,246 Individuals Selected from UK Biobank cohort

In the UK Biobank, there are about 500,000 participants in total. 392,246 of these individuals have ICD-10 codes in their records. For these patients, we selected 219,604, 86,361, and 86,361 unique

patients for training, validation, and testing respectively. The three sets have similar basic characteristics (Table 1). Fifty-six percent of individuals are women. The majority of participants are white. Elderly adults dominate the selected cohort with an average age of 71. We assessed 1,538 Phecode labels extracted from 12,803 ICD-10 codes from the cohort. Diagnostic labels have a long-tail distribution (Figure 2A): nearly 40% of these Phecode labels have fewer than 100 positive patients (Figure 2C). Among 392,246 individuals, 377,612 people have fewer than 30 phenotypes (Figure 2B). We integrate 38,663 category-specific features and summarize them into 20 data regimes as potential risk factors to aid our analysis (Table S1).

Table 1. Basic characteristics of the selected UK Biobank cohort

	Training set (N = 219,604)	Validation set (N = 86,321)	Test set (N = 86321)
Race, n%			
White	206,394 (93.985)	81,646 (94.584)	81,365 (94.259)
Mixed	1,304 (0.594)	478 (0.553)	497 (0.576)
Asian	3,489 (1.589)	1,394 (1.615)	1,364 (1.580)
Black	4,459 (2.030)	1,468 (1.701)	1,621 (1.878)
Chinese	728 (0.332)	159 (0.184)	213 (0.247)
Other	2,046 (0.932)	670 (0.776)	747 (0.865)
Unknown	690 (0.314)	293 (0.339)	325 (0.377)
Did not answer	494 (0.225)	213 (0.246)	189 (0.219)
Sex, n%			
Female	122,353 (55.715)	47,315 (54.813)	47,786 (55.358)
Male	97,251 (44.285)	39,006 (45.187)	38,535 (44.641)
Age, n%			
< 65 years	58,988 (59.447)	16,905 (59.472)	19,680 (59.449)

≥ 65 years	160,616 (74.378)	69,416 (75.381)	66,641 (74.946)
All	219,604 (70.367)	86,321 (72.266)	86,321 (71.413)

Phecode embeddings reflect disease similarity

Since POPDx addresses rare and unobserved diagnostic codes based on their textual description and the ontological relationship to common diseases, its performance relies on high quality embeddings of phenotypes. For that reason, we verified that diagnostic codes that are direct neighbors in the graph of Human Disease Ontology are also close in our low-dimensional embedding space. We compared three types of phenotype similarities: the disease ontology structure-based similarity, the text-based similarity, and joint semantic and structure-based similarity (**Methods**). We assessed the phenotype embeddings using direct neighborhood and non-direct neighborhood proximity. We first observe the average cosine distance of direct neighbors in the disease ontology graph is 0.15 ± 0.04 , which is 69.70 % higher than that of the text-based embeddings (0.05 ± 0.01), while the average cosine distance of k-hop neighbors (0.34 ± 0.02) in the disease ontology graph is 83.02% higher than those of the text-based embeddings (0.06 ± 0.01) (Figure 3B). The average cosine distances of joint embeddings in the same disease type neighborhood and k-hop neighborhood are 0.05 ± 0.01 and 0.07 ± 0.01 respectively (Figure 3C). POPDx incorporates the joint semantic and topology preserving embeddings under the principle that the unobserved or unseen phenotypes in training can borrow information from other disorders based on their shared characteristics.

Dimension reduction via *t*-distributed stochastic neighbor embedding (*t*-SNE) [18] on the joint semantic and structure-based embeddings reveals distinct disease groups (Figure 3A). The joint embeddings of Phecodes via a biomedical domain-specific pre-trained language model [19] and

canonical classification of the diagnoses present disjoint clusters in the low-dimensional embedding space (Figure 3A, Figure S4 A, B). Whereas diseases of most organ systems (Figure 3A, B) are independently clustered in latent space (for example, Diseases of the ear and mastoid process, Diseases of the eye and adnexa, Diseases of the circulatory system), some categories of diagnostic codes do not form a clear cluster but intermix (e.g., External causes of morbidity and mortality, Injury, poisoning and certain other consequences of external causes). To quantify the similarity of the Phecodes within and outside of the disease category, we measure the two types of dissimilarity of each disease class (Figure S2). The phenotype codes for pregnancy, childbirth, and the puerperium have the highest similarity with a mean in-group cosine distance of 0.04 ± 0.01 , in contrast with diseases of the musculoskeletal system and connective tissue that have the lowest in-group similarity with a mean in-group cosine distance of (0.08 ± 0.06) . The relationships are visualized in the dendrograms (Figure S3) which present the hierarchical relationship between our phenotypic embeddings for different disease categories. For example, phenotypes for the infectious and parasitic diseases (Figure S3A) form correlated groupings in the topological space, such as 41.1 and 41.2 (staphylococcus and streptococcus infections).

Improved disease recognition for unseen, rare, and common phenotypes

To evaluate the performance of POPDx on different phenotypes, we categorize phenotypes according to the number of instances in the training set (Figure 4). Most diagnostic labels (98.7%) have fewer than 1000 patient samples (Figure 2B). POPDx (Figure 4, S6) yields AUROC (Area Under the Receiver Operating Characteristic Curve) scores of 0.71 and 0.74 for phenotypes with 0-10 and 10-100 training samples. The AUROC and AUPRC (Area Under the Precision-Recall Curve) scores improve with training size. We also investigated performance for phenotypes with no patient sample in the training dataset. For these, POPDx achieves an AUROC score of 0.68 and

an AUPRC score of 0.24, which are 74% and 218% higher than those of the logistic regression baseline. A sampling ratio of positive to negative patients of 1:10 is consistently used to report the AUROC and AUPRC of all the experiments.

Across different disease categories of phenotypes, we investigate how well POPDx outperforms the baseline of logistic regression based on AUROC and AUPRC scores (Figure 5A, B). We achieve an AUROC of 0.81 and an AUPRC of 0.37 with 131 phenotypes for Diseases of the circulatory system (Table 1). We outperform the random forest and logistic regression for increases in AUROC and AUPRC scores by 0.16 and 0.15. We compared POPDx with other strategies for phenotype embedding (Figure 4, Figure 4S). The joint semantic and structure-based embedding method achieves the best performance compared to NLP-based and ontology-based frameworks. Interestingly, for phenotypes that have fewer than 100 patient samples, the NLP-based and ontology-based frameworks improve the AUROC and AUPRC scores compared to those of random forest and logistic regression. To assess the ability of POPDx to work with even larger sets of phenotypes, we applied patient phenotyping across 12,803 ICD-10 diagnostic codes (almost 10 times more codes than with Phecodes) with the same dataset. POPDx detects diagnostic labels for both rare and common codes with competitive AUROC scores (Figure 5S).

Table 2. AUROC and AUPRC scores of different disease categories

Disease Category (Abbrev.)	AUROC		AUPRC	
	Mean	Std	Mean	Std
(PERIN) Certain conditions originating in the perinatal period	0.6859	0.1669	0.2606	0.2253
(ID) Certain infectious and parasitic diseases	0.7215	0.1106	0.2793	0.1318
(CONGEN) Congenital malformations, deformations and chromosomal abnormalities	0.6403	0.1686	0.1953	0.1156

(BLOOD)				
Diseases of the blood and blood-forming organs and certain disorders involving the immune mechanism	0.7520	0.0649	0.2851	0.1105
(CV) Diseases of the circulatory system	0.8141	0.0725	0.3695	0.1238
(GI) Diseases of the digestive system	0.7913	0.0887	0.3621	0.1495
(EAR) Diseases of the ear and mastoid process	0.7561	0.1007	0.3179	0.1598
(EYE) Diseases of the eye and adnexa	0.7642	0.0762	0.3132	0.1103
(GU) Diseases of the genitourinary system	0.7902	0.0765	0.3252	0.1177
(MSK) Diseases of the musculoskeletal system and connective tissue	0.7423	0.0982	0.2819	0.1285
(NEURO) Diseases of the nervous system	0.7560	0.0849	0.3232	0.1592
(RESP) Diseases of the respiratory system	0.8113	0.0700	0.3886	0.1434
(SKIN) Diseases of the skin and subcutaneous tissue	0.6995	0.1149	0.2439	0.1392
(ENDO) Endocrine, nutritional and metabolic diseases	0.7633	0.1135	0.3234	0.1366
External causes of morbidity and mortality	0.7226	0.0979	0.2934	0.1053
Factors influencing health status and contact with health services	0.7591	0.0960	0.3077	0.1427
(EXT) Injury, poisoning and certain other consequences of external causes	0.7378	0.0657	0.2684	0.0930
(BEH) Mental and behavioural disorders	0.7656	0.0859	0.3175	0.1452
(NEO) Neoplasms	0.7571	0.0826	0.3028	0.1208
(GYN) Pregnancy, childbirth and the puerperium	0.9282	0.0856	0.6344	0.1879
(LAB) Symptoms, signs and abnormal clinical and laboratory findings, not elsewhere classified	0.7375	0.0779	0.2609	0.0903
(RHEU) Systemic connective tissue disorders	0.7334	0.0915	0.2730	0.1231

Explaining output of POPDx

Scoring the importance of individual features provides some interpretability for model predictions. We computed feature relevance scores over 1,538 phenotypes using DeepLIFT (**Method**). We analyze feature importance for individual predictions. We visualize the essential features with a polar plot that is organized into 20 data regimes (Table S1). For the phenotype atherosclerosis

(440.0 Diseases of arteries, arterioles, and capillaries), Figure 6A shows a polar chart for three true-positive patients, who share a similar pattern of feature importance. In particular, features from medical history, physical measure, education and employment status, and physical measure are important. Figure 6B shows 5 categories of diseases for which we computed the max value of the importance scores of the selected data regimes. Features in the lifestyle regime are critical for the recognition of endocrine, nutritional, and metabolic diseases. The medical history regime is important for the recognition of phenotypes originating in the perinatal period. For the external causes of morbidity and mortality, the features related to mental health status are essential.

METHODS

The POPDx framework leverages Phecode embeddings that are constructed from the Human Disease Ontology and the textual descriptions of the Phecodes to achieve simultaneous recognition of multi-phenotype that outperform the state-of-the-art models. We assessed our embeddings by computing the dissimilarity of phenotypes within and outside of the disease category. The importance scores of 38,663 features were evaluated to aid the POPDx explainability.

UK Biobank cohort

We extracted phenotypic and health-related information from the UK Biobank including clinical assessments, lifestyle questionnaires, physical measurements, and electronic medical records. Among approximately 500,000 individuals from the UK Biobank dataset, 392,246 individuals have ICD-10 coded diagnosis information. We binned and applied one-hot encoding to numerical and categorical features, respectively, into 38,663 binary variables. For 1,538 diagnostic labels, we map 12,803 International Classification of Diseases Tenth Revision (ICD-10) codes to 1,538 Phecodes [20]. The entire dataset was split into training, validation, and test sets. Instead of

dividing the data randomly, we split the individuals to allow experimental evaluation of unseen, rare, and common diseases. We generated a large multi-label patient dataset to contain Phecodes that are present or absent in the training dataset. Some Phecodes occur zero or a few times to simulate unseen and rare diseases while others are common.

The joint semantic and structure-based embeddings of phenotypes

We relied on both the textual information and hierarchical tree-structure of the phenotypes to compute the joint semantic and structure-based embeddings of Phecodes. The Phecode embeddings depend on embeddings of the ICD-10 codes which comprise them. We downloaded the hierarchical tree-structured representation of the ICD-10 data from the online showcase of UK Biobank resources. We use the hierarchical relation of the ICD-10 codes to construct an undirected network of phenotypes. There are 19,155 nodes in the network, corresponding to 19,155 codes. Edges are not weighted. We perform a shortest-path graph search and then compute the low-dimensional representation of each diagnostic code by using the singular value decomposition (SVD) [21]. We thus have a compressed, low-dimensional representation of each ICD-10 code based on the undirected disease network.

The text description of each ICD-10 code is a sentence or a short term that characterizes the meaning of the code. For example, ICD-10 code P29 is described as “*Cardiovascular disorders originating in the perinatal period*”. We use the pre-trained version of the BioBERT [19] model to extract fixed vector of ICD-10 code based on this text. The BERT [19, 22] model breaks down the textual description of each ICD-10 code into tokens. Then, it adds a special classification token [CLS] at the beginning of each text. The 768-dimensional hidden state embedding of the "[CLS]" token from the last layer is used as the aggregate representation for the ICD-10 code. Finally, we merge the final two representations from NLP-mapping and network-based embeddings of disease

terms. Given the ICD-10 codes and the vector representation of their textual description, we can calculate the embedding for each Phecode by averaging the representations of the ICD-10 codes to which the Phecode corresponds. We included 12,803 ICD-10 codes present in our UK Biobank dataset which map to 1,538 Phecode labels. (Figure 1B, C).

Calculating phenotype dissimilarity

We compute three measures of Phecode dissimilarity based on the disease ontology embedding, the embedding of the associated text, and both together. We measure the distance between embeddings with cosine distance. The distances are calculated as in-group (intra-) and out-group (inter-) distances. The cosine distances between a phenotype and those within the same disease category are considered in-group dissimilarity. The cosine distances between phenotypes of different disease categories are computed as out-group dissimilarity.

Simultaneous recognition of Multiple-phenotypes

Our algorithm (Figure 1B) leverages the text description and ontological relationships of phenotypes to predict novel phenotypes (with no training examples) by relating them to clinically and contextually similar phenotypes. We use a bilinear model to predict the disease type for both seen and unseen phenotypes. Let P be an $m \times n$ matrix of input embedding of the patients, where m is the number of patients and n is the number of features. Let Y be an $m \times c$ label matrix, where c is the total number of phenotypes. $Y_{ij}=1$ if patient i has a diagnostic label of phenotype j , otherwise $Y_{ij}=0$. c is the total number of Phecodes, and the majority of these phenotypes have fewer than 1000 examples in the training data. For example, when a patient is associated with 126 disease labels, the corresponding columns of diseases are ones while the others were all zeros in the label matrix. Let U be a $c \times h$ matrix of the low-dimensional representations of disease types,

where h is 1,268, the dimension of phenotype embedding space. We optimize the following binary cross-entropy loss:

$$\sum_{i=1}^m \sum_{j=1}^c \left[Y_{ij} \log \sigma(P_i W_1 W_2 U_j^T) + (1 - Y_{ij}) \log (1 - \sigma(P_i W_1 W_2 U_j^T)) \right]$$

where $W_1 \in \mathbb{R}$ dimensionality is set to be 150 through parameter tuning. POPDx optimizes the objective function by Adam optimizer. After the optimization, the likelihood of a diagnostic code j presented by a patient with a feature vector p is estimated as

$$L_j = \text{Sigmoid}(p W_1 W_2 U_j^T)$$

where L_j is the probability that the phenotype j belongs to this patient. $L = \{L_1, L_2, \dots, L_{1538}\}$ is the probability distribution of diagnosis labels for a patient. We use Pytorch [23], Matplotlib [24], and Numpy [25] for the experiments.

Feature importance analysis

We use DeepLIFT to calculate the importance and relevance of 38,663 features on each of the 1,538 phenotypes. DeepLift is a backpropagation algorithm that measures the contribution of individual features on the output of a neural net for a specific input [26]. It computes the differences between the activation of each neuron and their reference activation, where the “reference” is computed based on the selected negative samples. DeepLIFT highlights both positive (supportive) and negative (not supportive) influences on the prediction. The magnitude of the relevance value corresponds to its importance. We implemented DeepLIFT in the framework Captum [27]. First, DeepLIFT scores are computed for each feature and for each patient. Then, for each phenotype, the DeepLIFT scores of all the true-positive patient data are averaged to obtain an importance score for each feature. We create a vector of feature importance scores for each phenotype.

DISCUSSION

As large databases of patient records become available for research, associating precise phenotypes with patients becomes critical. Our method comprehensively and simultaneously scores hundreds to thousands of phenotypes. Automated phenotyping of a patient, even for a single disease, faces two central challenges: variations in the syntax and semantics of health records (different electronic systems, lack of standards for interoperability among hospitals, etc.), and patient-to-patient variability in the clinical manifestations of the diseases [28, 29]. Most existing computational approaches to phenotype recognition are built by hand and model a small number of clinical, pathological, and laboratory attributes of patients [30, 31]. These methods do not easily generalize to cover the whole disease ontology [32, 33]. In addition, no methods using machine learning have been able to recognize phenotypes for which there are new or no training examples in the UK Biobank. Our integrated analysis allows us to make some progress in recognizing such examples.

The UK Biobank cohort is a long-tailed dataset with heavy class imbalance (Figure 2A). POPDx provides robust and scalable recognition of phenotypes; it performs quite well on common phenotypes for which there are many examples, and gracefully degrades its performance down to phenotypes with zero examples. The ROC curves (Figure S6) display the trade-off between sensitivity and specificity and can be helpful when considering the cut-off threshold to identify the diseased cohorts. The AUPRC (Figure 4) is prevalence dependent and less optimistic when the phenotype prevalence is low. Our framework significantly improved the AUPRC for unseen and rare phenotypes (<10 cases in training) by 218% and 151% compared to the logistic regression model. If a clinical team wants to identify patients for a phenotype with very low prevalence, our model on average doubled the ability to find the positive cases in the UK Biobank. When high

specificity is desired over sensitivity in a clinical setting, more expert filtering can be used to detect the false positives. Our model provides a better starting point for the clinicians. This is encouraging since POPDx makes rare disease imputation feasible. Our method takes advantage of the non-linear correlation structure of the patient features to assign multiple diagnostic labels. In contrast, conventional machine learning methods such as random forest are unable to recognize phenotypes that are not present in the training dataset, inevitably limiting their applications in recognition of new phenotypes.

Our framework incorporates structural knowledge of the disease ontology by embedding disease relationships in a low-dimensional space. The recognition of unseen and rare phenotypes is enabled by explicitly providing information about the network relationships of these phenotypes to others which are well-represented in our data set. This phenotype ontology embedding preserves proximity relations, so two representations of nearby phenotypes are embedded in similar locations. In addition to the disease ontology, our method leverages semantic information about phenotypes by including textual information (embedded by BioBERT [19]) that provides further context for the phenotype and its distance from other phenotypes. Either the NLP-based or ontology-based embedding provide meaningful correlations of the phenotypes which can be demonstrated by their competitive performance in recognizing uncommon conditions. The combination of structure-based representations from the disease ontology with the contextual embeddings of phenotype text descriptions provides complementary information. The t-SNE representations (Figure 3A) of the joint embeddings demonstrate that our method preserves the separations of major disease types.

With reliable identification of patients with phenotypes, we can use the genotype information present in the UK Biobank to seek genetic associations. We can also use known genetic associations between phenotypes to add an additional element to our embedding to help with

phenotype recognition (i.e., a third element to our embedding in addition to the text and ontology structure). Our results demonstrate that our model’s DeepLIFT feature relevance scores [26] can offer some insights to explain the assignment of 1,538 phenotypes. Our results with DeepLIFT show promise but they may not provide sufficiently clear justification for the reasons a feature contributes to a phenotype. For example, chest pain felt outside physical activity has a high importance score for the Phecode 335.0 (hereditary/degenerative nervous conditions). While this may be reasonable, the mechanistic connection between these concepts is not clear.

The algorithm is implemented in Python (<https://github.com/luyang-ai4med/POPDx>). The UK Biobank dataset is anonymized and only available through approved access (<https://www.ukbiobank.ac.uk/>).

CONCLUSIONS

The POPDx framework was developed for multi-phenotype recognition with heterogeneous patient data in the UK Biobank. Our model outperforms other existing methods on recognizing a comprehensive set of non-existent, rare, and common phenotypes in training. While we demonstrate our framework on UK Biobank, the model can be applied to any biobank-related records.

ACKNOWLEDGEMENTS

RBA is supported by NIH GM102365 and Chan-Zuckerberg initiative. LY is supported by Agilent and the Chan-Zuckerberg Biohub. We would like to thank Stanford sherlock cluster for high-performance computing (HPC) and access to the long-term data storage through the OAK research filesystem and compute nodes (GPUs, CPUs).

FIGURES

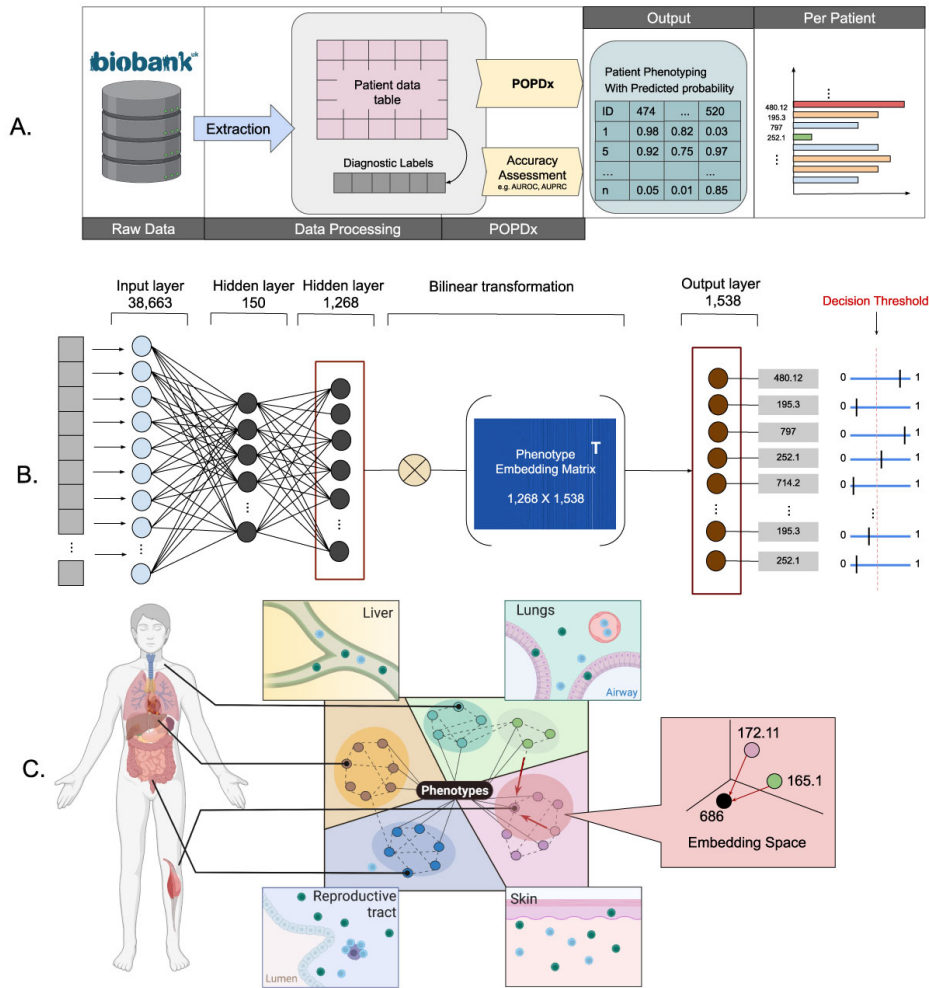


Figure 1. POPDx overview. (A) The flowchart of patient phenotyping in UK Biobank includes raw data extraction, data processing, POPDx development, and result evaluation. After extracted and preprocessed the raw data from UK Biobank, we obtained vectors of features for all patients as shown in the patient data table and a vector of diagnostic labels of Phecodes for each patient. We developed POPDX to encode the patient features that are eventually used to perform phenotype recognition. The output of POPDx is a matrix of probabilities which represents the likelihoods of all Phecodes for all the patients. We evaluated the accuracy of POPDx by AUROC and AUPRC. (B) The architecture of POPDx is a bilinear model that leverages an embedding matrix of 1,538 Phecodes. A total number of 38,663 features per patient were input into POPDx. The structure of POPDx includes an input layer, two hidden layers each with 150 and 1,268 neurons, and a bilinear transformation through an embedding matrix of the phenotypes. The output layer is the probability distribution that this patient is assigned with each Phecode label. The Phecode labels are either 0 or 1 based on the decision threshold, illustrated as the vertical dashed line. (C) POPDx embeds the phenotypes into low-dimensional space. The hierarchical tree-structured representation of the phenotypes is utilized. For simplicity, we only show 4 categories of diseases. Even if the Phecode does not have any patient examples in the training data, POPDx can leverage its relation to other Phecodes in the embedding space. Figure adapted from “Distribution of TRM Cells”, by BioRender.com (2022). Retrieved from <https://app.biorender.com/biorender-templates>.

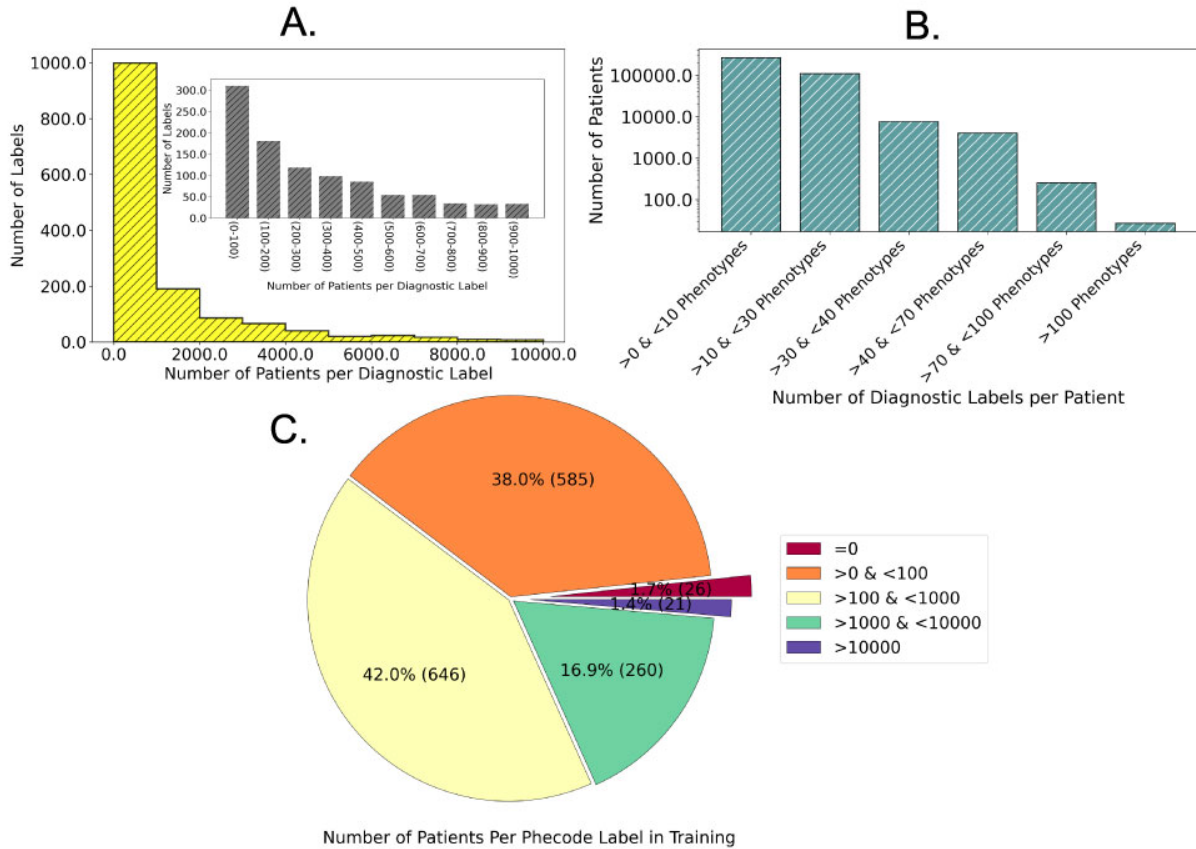


Figure 2. Diagnostic label statistics. (A) The UK Biobank has a long-tailed distribution of Phecode labels. The x-axis is the number of patients per Phecode Label and y-axis is the number of labels. Most of the Phecode labels have fewer than 1000 patients in the UK Biobank. (B) The patients in UK Biobank are associated with multiple phenotype labels. The x-axis is the groups of Phecode counts and log-scale y-axis is the number of patients. The majority of the patients have fewer than 30 Phecodes labels. (C) The phenotypes are categorized based on the number of training samples. The exploded pie chart shows the relative abundance of Phecodes based on the number of patients in training.

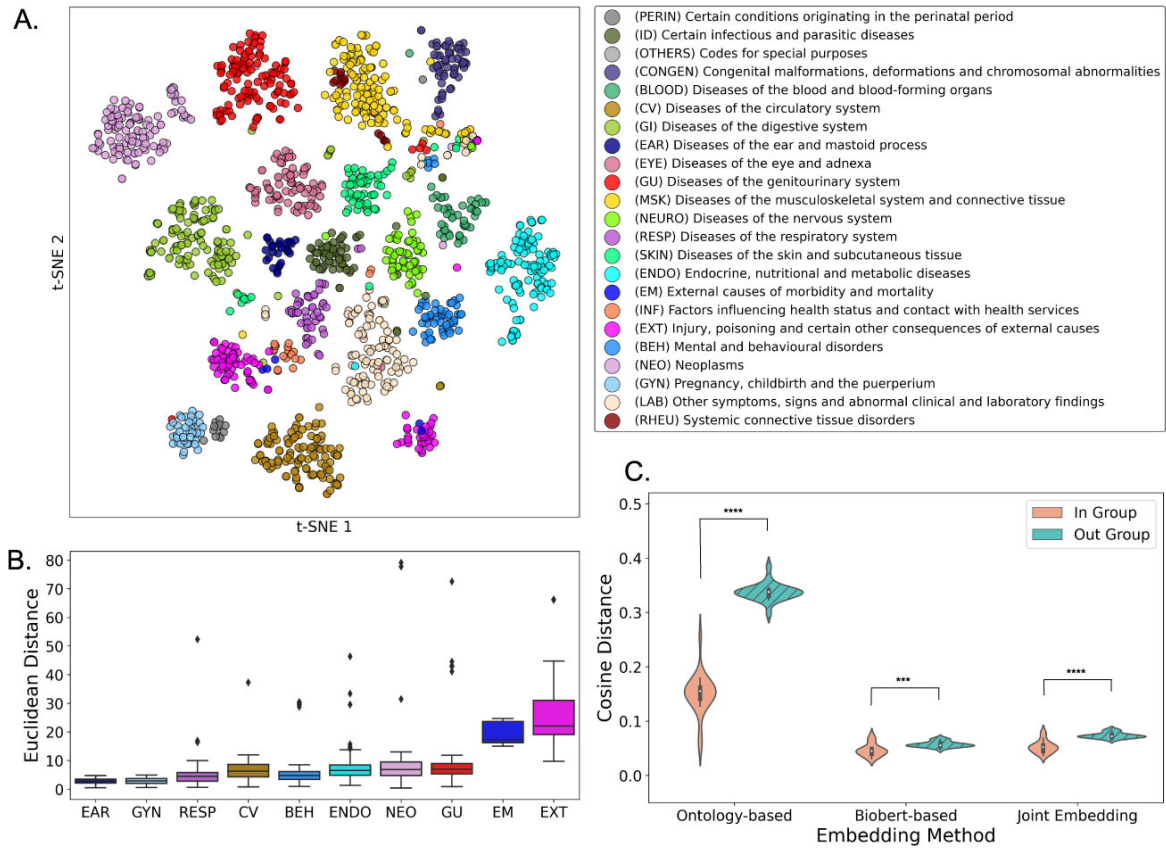


Figure 3. Phenotype embeddings. (A) The *t*-SNE plot shows the segregation of phenotypes into different disease categories using the joint structure and semantic embedding method. The legend associates a color to each phenotype category based on the hierarchical tree-structure of ICD-10. (B) The Euclidean distance of Phecodes to the cluster center of each disease category in the *t*-SNE plot. (C) The similarity analysis of phenotype groups embedded with three different methods is presented as cosine differences within groups and between groups.

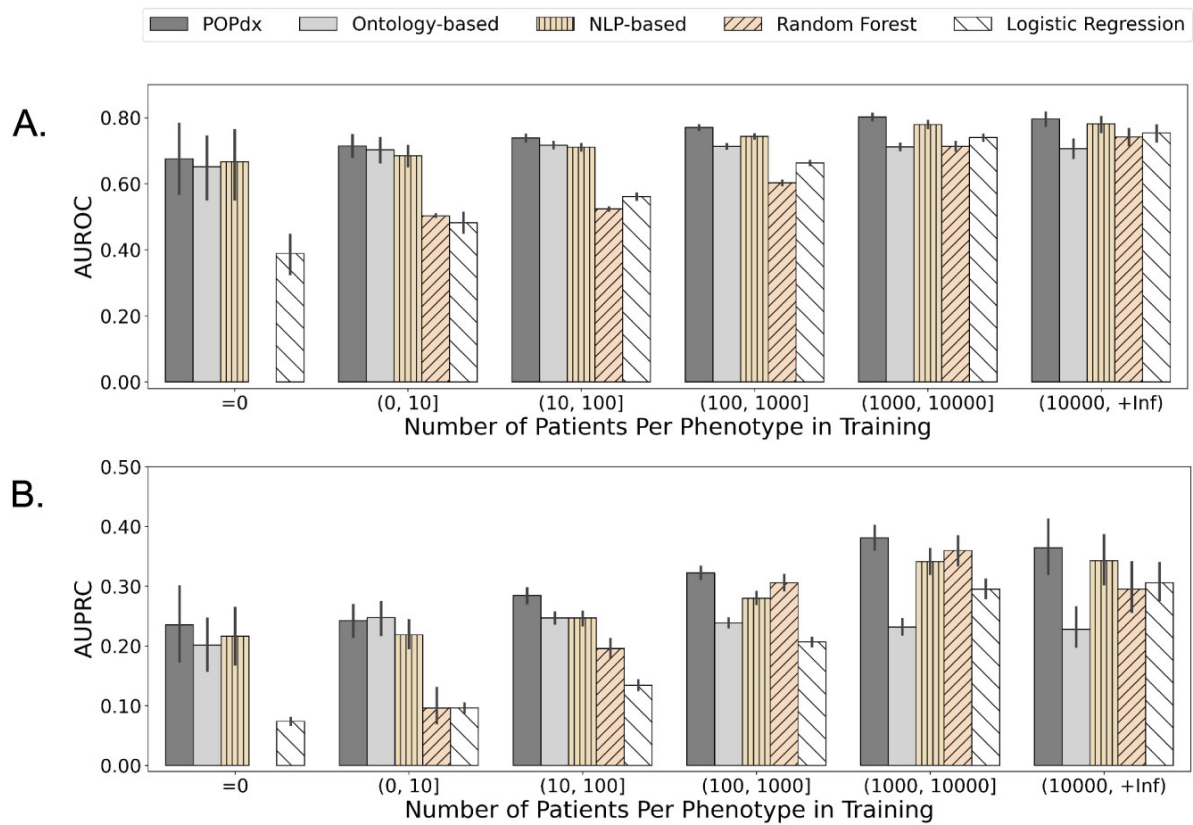


Figure 4. POPDx can recognize phenotypes that are not present in the training set. Bar plots comparing POPDx and other methods in terms of (A) AUROC and (B) AUPRC on the test set. POPDx presents competitive performance across all the groups of phenotypes.

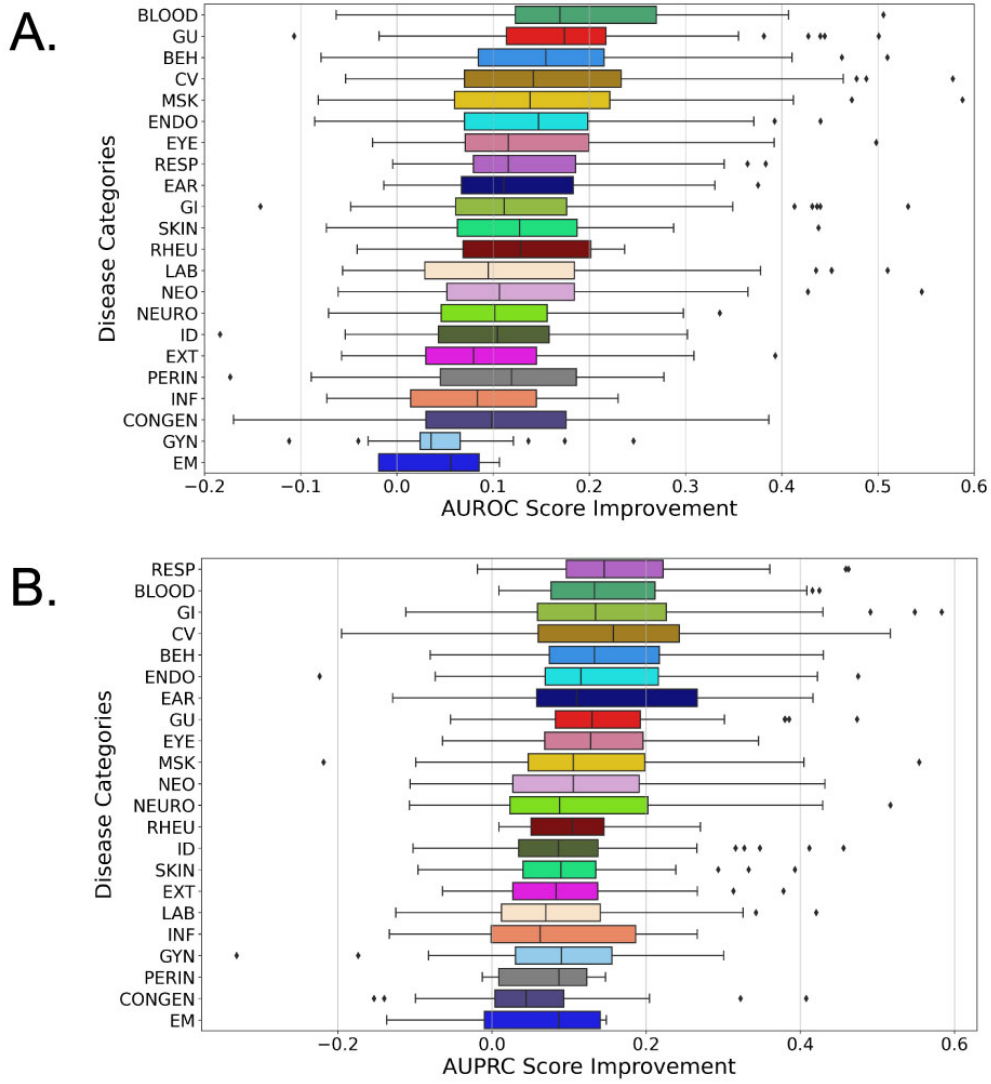


Figure 5. POPDx improves disease recognition compared with logistic regression across 22 disease categories. (A) The AUROC scores for all the disease categories are substantially improved compared to the logistic regression (LR) baseline. The x-axis is the improvement of AUROC score by POPDx. The y-axis represents different disease categories. (B) The AUPRC scores for all the disease categories are substantially improved compared to the logistic regression (LR) baseline. The x-axis is the improvement of AUPRC score by POPDx. The y-axis represents different disease categories.

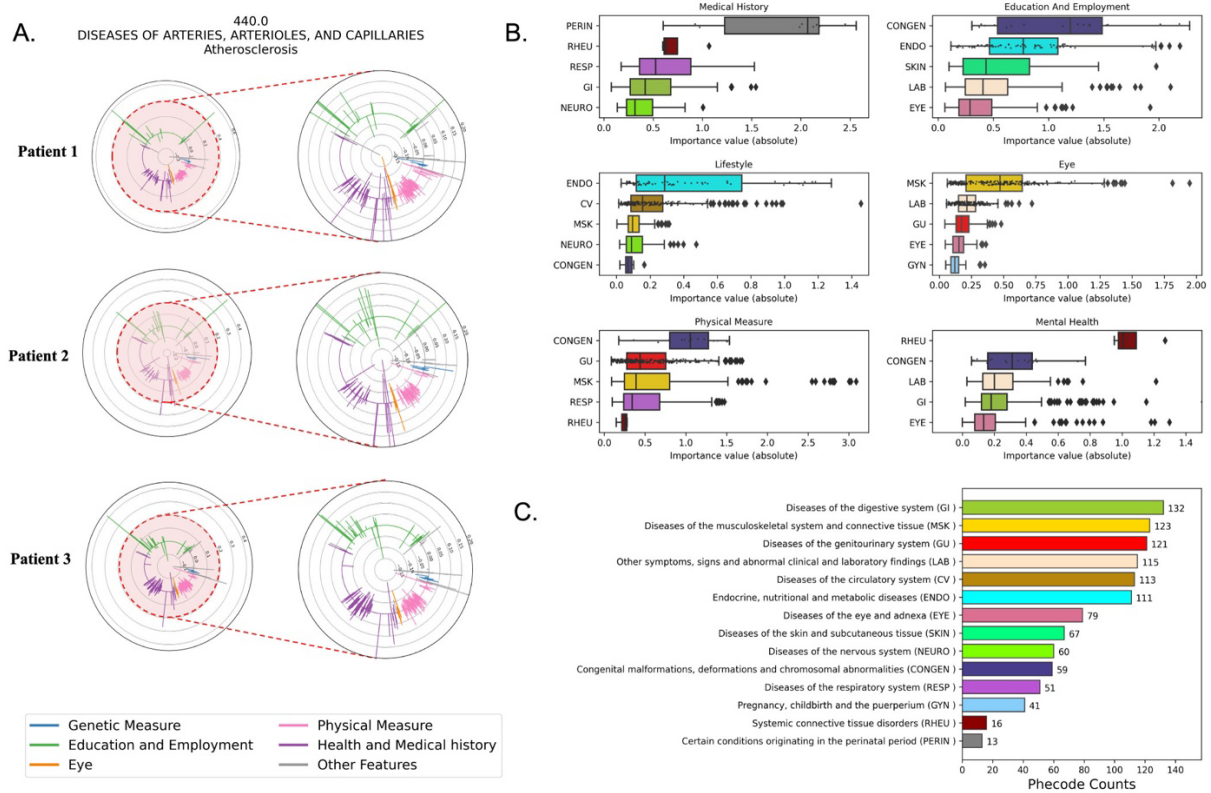


Figure 6. POPDx explainability across different disease categories. (A) Feature relevance profile for phenotype 440.0. The polar plots summarize feature importance for three true-positive patients with atherosclerosis. The polar plots on the right represent the zoomed-in region as highlighted in red to aid the eye. The legend associates a line color to a feature regime. Radial values in the polar plots are feature importance magnitude from DeepLIFT. All features are analyzed into different regimes to show the consistency of the POPDx interpretability. (B) Additive contributions of individual features (medical history, education and employment, lifestyle, eye, physical measure, mental health shown here) to the outputs of POPDx. Each color is associated with a disease category which is consistent with the colors of disease categories in panel C. X-axis specifies the importance value of the corresponding feature regimes (higher importance to the right). Y-axis is 5 disease categories sampled based on the median importance values from DeepLIFT. (C) A horizontal bar plot of the number of Phecodes in the disease

categories. The colors in (B) and (C) are consistently used to represent different categories of phenotypes.

REFERENCES

1. Rajpurkar, Pranav, et al. "Chexnet: Radiologist-level pneumonia detection on chest x-rays with deep learning." *arXiv preprint arXiv:1711.05225* (2017).
2. Ford, Elizabeth, et al. "Extracting information from the text of electronic medical records to improve case detection: a systematic review." *Journal of the American Medical Informatics Association* 23.5 (2016): 1007-1015.
3. Ting, Daniel Shu Wei, et al. "Artificial intelligence and deep learning in ophthalmology." *British Journal of Ophthalmology* 103.2 (2019): 167-175.
4. LaPierre, Nathan, et al. "MetaPheno: A critical evaluation of deep learning and machine learning in metagenome-based disease prediction." *Methods* 166 (2019): 74-82.
5. Krittanawong, Chayakrit, et al. "Artificial intelligence in precision cardiovascular medicine." *Journal of the American College of Cardiology* 69.21 (2017): 2657-2664.
6. Bycroft, Clare, et al. "The UK Biobank Resource with Deep Phenotyping and Genomic Data." *Nature*, vol. 562, no. 7726, 2018, pp. 203–209., doi:10.1038/s41586-018-0579-z.
7. Xiao, Cao, et al. "Opportunities and Challenges in Developing Deep Learning Models Using Electronic Health Records Data: a Systematic Review." *Journal of the American Medical Informatics Association*, vol. 25, no. 10, 2018, pp. 1419–1428., doi:10.1093/jamia/ocy068.
8. Shickel, Benjamin, et al. "Deep EHR: A Survey of Recent Advances in Deep Learning Techniques for Electronic Health Record (EHR) Analysis." *IEEE Journal of Biomedical and Health Informatics*, vol. 22, no. 5, 2018, pp. 1589–1604., doi:10.1109/jbhi.2017.2767063.

9. Zhang, Xiaoqing, et al. "A novel deep neural network model for multi-label chronic disease prediction." *Frontiers in genetics* 10 (2019): 351.
10. Tafa, Zhilbert, Nerxhivane Pervetica, and Bertran Karahoda. "An intelligent system for diabetes prediction." *2015 4th Mediterranean Conference on Embedded Computing (MECO)*. IEEE, 2015.
11. Huang, Mu-Jung, Mu-Yen Chen, and Show-Chin Lee. "Integrating data mining with case-based reasoning for chronic diseases prognosis and diagnosis." *Expert systems with applications* 32.3 (2007): 856-867.
12. Nguengang Wakap, Stéphanie, et al. "Estimating cumulative point prevalence of rare diseases: analysis of the Orphanet database." *European Journal of Human Genetics* 28.2 (2020): 165-173.
13. Schaefer, Julia, et al. "The use of machine learning in rare diseases: a scoping review." *Orphanet Journal of Rare Diseases* 15.1 (2020): 1-10.
14. Horn, Werner. "AI in medicine on its way from knowledge-intensive to data-intensive systems." *Artificial Intelligence in Medicine* 23.1 (2001): 5-12.
15. Budysh, Karolina, Thomas M. Helms, and Carsten Schultz. "How do patients with rare diseases experience the medical encounter? Exploring role behavior and its impact on patient–physician interaction." *Health policy* 105.2-3 (2012): 154-164.
16. Wang, Sheng, et al. "Unifying Single-Cell Annotations Based on the Cell Ontology." 2019, doi:10.1101/810234.
17. Brbić, Maria, et al. "MARS: discovering novel cell types across heterogeneous single-cell experiments." *Nature Methods* 17.12 (2020): 1200-1206.

18. Maaten, Laurens van der, and Geoffrey Hinton. "Visualizing data using t-SNE." *Journal of machine learning research* 9.Nov (2008): 2579-2605.
19. Lee, Jinhyuk, et al. "BioBERT: a Pre-Trained Biomedical Language Representation Model for Biomedical Text Mining." *Bioinformatics*, 2019, doi:10.1093/bioinformatics/btz682.
20. Wu, Patrick, et al. "Mapping ICD-10 and ICD-10-CM codes to phecodes: workflow development and initial evaluation." *JMIR medical informatics* 7.4 (2019): e14325.
21. Wall, Michael E., Andreas Rechtsteiner, and Luis M. Rocha. "Singular value decomposition and principal component analysis." *A practical approach to microarray data analysis*. Springer, Boston, MA, 2003. 91-109.
22. Devlin, Jacob, et al. "Bert: Pre-training of deep bidirectional transformers for language understanding." *arXiv preprint arXiv:1810.04805* (2018).
23. Paszke, Adam, et al. "Pytorch: An imperative style, high-performance deep learning library." *Advances in neural information processing systems* 32 (2019).
24. Hunter, John D. "Matplotlib: A 2D graphics environment." *Computing in science & engineering* 9.03 (2007): 90-95
25. Van Der Walt, Stefan, S. Chris Colbert, and Gael Varoquaux. "The NumPy array: a structure for efficient numerical computation." *Computing in science & engineering* 13.2 (2011): 22-30.
26. Shrikumar, Avanti, Peyton Greenside, and Anshul Kundaje. "Learning important features through propagating activation differences." *International conference on machine learning*. PMLR, 2017.
27. Kokhlikyan, Narine, et al. "Captum: A unified and generic model interpretability library for pytorch." *arXiv preprint arXiv:2009.07896* (2020)

28. Palmer, Adam C., and Peter K. Sorger. "Combination cancer therapy can confer benefit via patient-to-patient variability without drug additivity or synergy." *Cell* 171.7 (2017): 1678-1691.
29. Middleton, Blackford, et al. "Enhancing patient safety and quality of care by improving the usability of electronic health record systems: recommendations from AMIA." *Journal of the American Medical Informatics Association* 20.e1 (2013): e2-e8.
30. Saranya, G., and A. Pravin. "A comprehensive study on disease risk predictions in machine learning." *International Journal of Electrical and Computer Engineering* 10.4 (2020): 4217.
31. Long, Erping, et al. "An Artificial Intelligence Platform for the Multihospital Collaborative Management of Congenital Cataracts." *Nature Biomedical Engineering*, vol. 1, no. 2, 2017, doi:10.1038/s41551-016-0024.
32. Goh, Kwang-Il, et al. "The human disease network." *Proceedings of the National Academy of Sciences* 104.21 (2007): 8685-8690.
33. Schriml, Lynn M., et al. "Human Disease Ontology 2018 update: classification, content and workflow expansion." *Nucleic acids research* 47.D1 (2019): D955-D962.

Supplemental

Table S1. Feature categories

Regime	Category	Count	Sum
Medical history	Summary Operations	5527	13795
	Medical conditions	2377	
	Death register	2008	
	Cancer register	1528	
	Operations	1216	
	Summary Administration	937	
	Claudication and peripheral artery disease	43	
	Pain	42	
	Medical information	36	
	General health	20	
	Chest pain	16	
	Stroke outcomes	12	
	Cancer screening	8	
	Sleep	8	
	Myocardial infarction outcomes	6	
Sexual factors	6		
Ongoing characteristics	5		
Education and Employment	Employment	10105	11739

	Employment history	1619	
	Education	15	
Physical measure	Autorefracton	3397	5807
	Acceleration intensity distribution	550	
	Acceleration averages	409	
	Body composition by impedance	352	
	Accelerometer calibration	177	
	Body size measures	161	
	Carotid ultrasound	144	
	Physical activity	138	
	Spirometry	136	
	Accelerometer wear time duration	89	
	Raw accelerometer statistics	88	
	ECG during exercise	57	
	MET Scores	38	
	Arterial stiffness	34	
	Hand grip strength	26	
	Breathing	8	
ECG at rest, 12-lead	3		
Medication	Medications	3709	3721

	Cannabis use	12	
Mental health	Mental health	192	605
	Depression	125	
	Anxiety	112	
	Self-harm behaviors	40	
	Unusual and psychotic experiences	37	
	Mania	26	
	Mental distress	26	
	Summary Psychiatric	24	
	Happiness and subjective well-being	23	
Genetic measure	Genotyping process and sample QC	588	588
Lifestyle	Diet	155	575
	Residential air pollution	134	
	Household	67	
	Electronic device use	59	
	Residential noise pollution	55	
	Sun exposure	34	
	Social support	32	
	Sleep	22	
	Other sociodemographic factors	12	

	Diet by 24-hour recall	3	
	Ongoing characteristics	2	
Biological sample	Blood count	313	355
	Blood sample collection	22	
	Saliva sample collection	8	
	Urine sample collection	8	
	Urine processing	4	
Eye	Intraocular pressure	115	269
	Eyesight	64	
	Visual acuity	55	
	Eye surgery/complications	35	
Early Life	Early life factors	244	244
Addiction	Smoking	117	165
	Addictions	43	
	Medical information	5	
Cognitive assessment	Fluid intelligence / reasoning	92	142
	Reaction time	20	
	Prospective memory	17	
	Numeric memory	6	
	Procedural metrics	4	

	Word production	3	
Women health	Summary Maternity	88	131
	Female-specific factors	43	
Family history	Family history	124	124
Traumatic history	Traumatic events	114	114
Baseline characteristics	Reception	66	113
	Baseline characteristics	25	
	Ethnicity	22	
Alcohol	Alcohol use	56	103
	Alcohol	47	
Hearing	Hearing	43	43
Men health	Male-specific factors	16	16
Mouth	Mouth	14	14

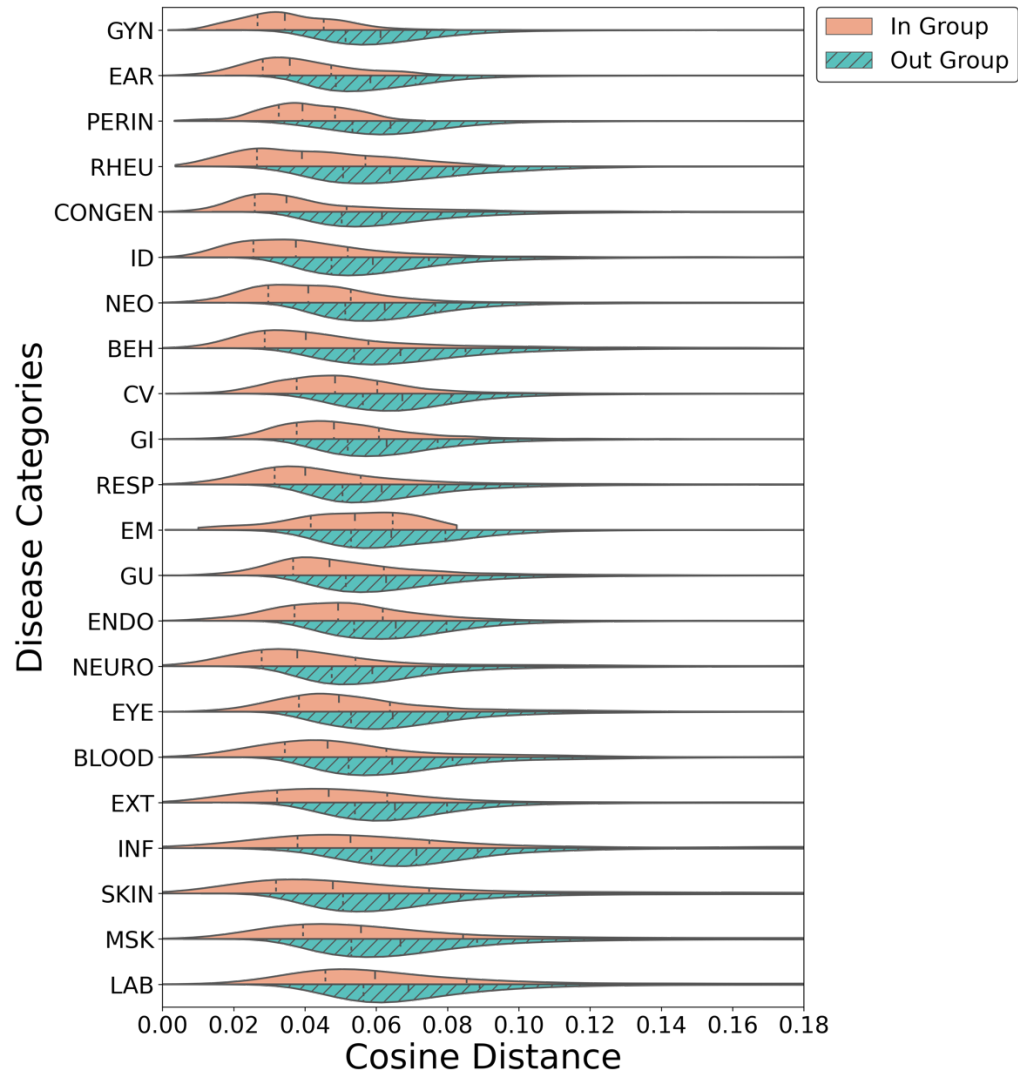
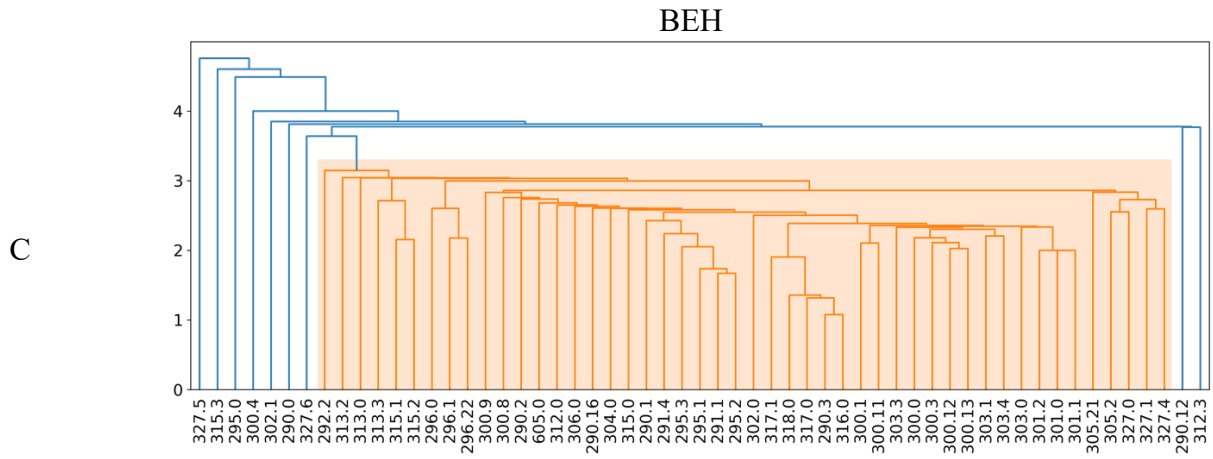
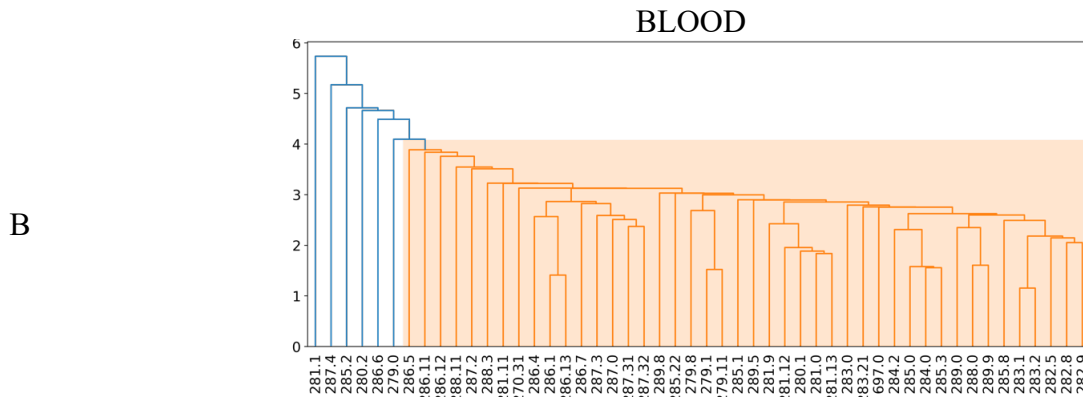
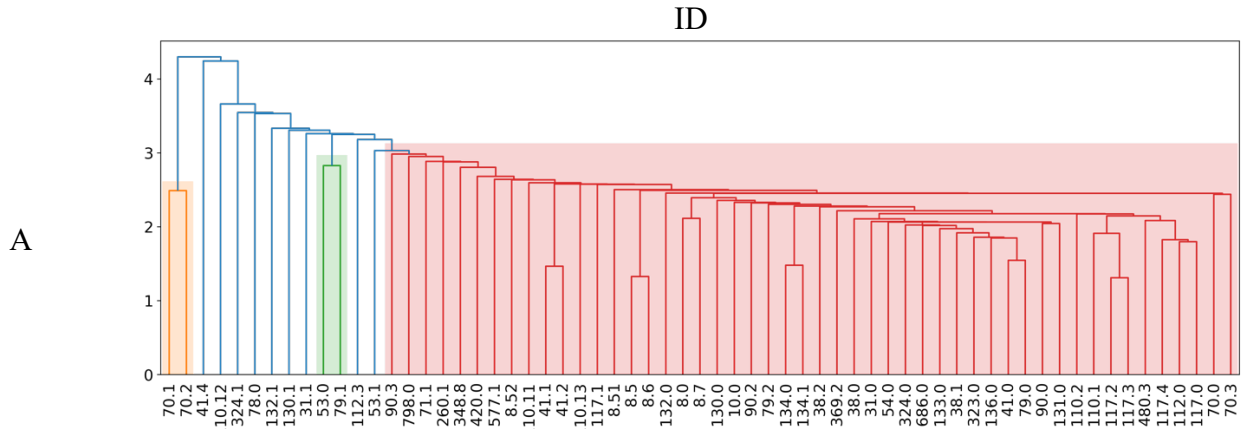
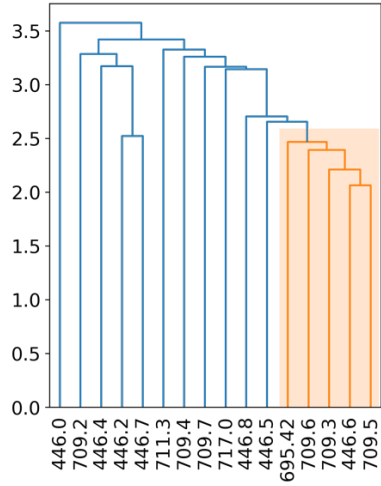


Figure S2. Phenotypes dissimilarity analysis across different disease categories. The cosine distances of phenotypes in different disease categories are represented as in-group (intra-) and out-group (inter-) distances.

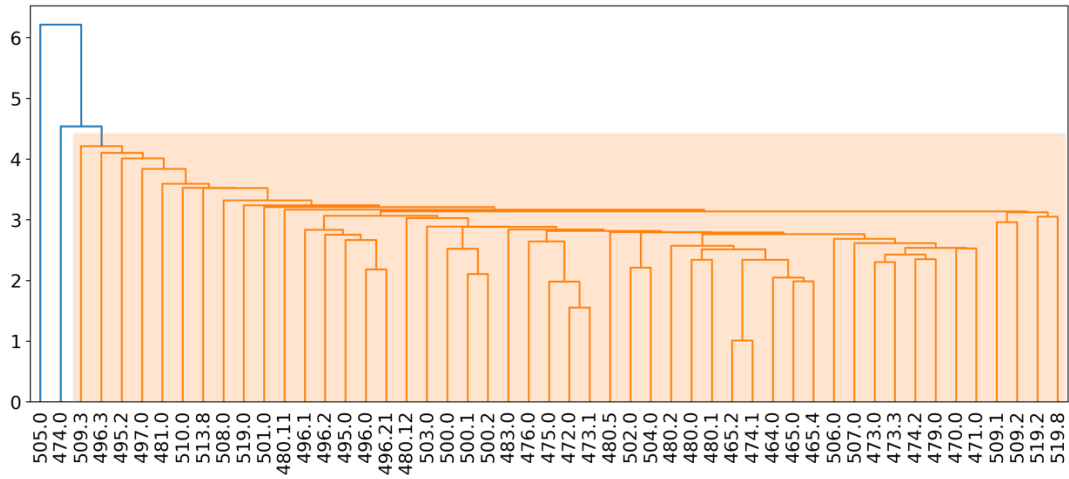


D

RHEU

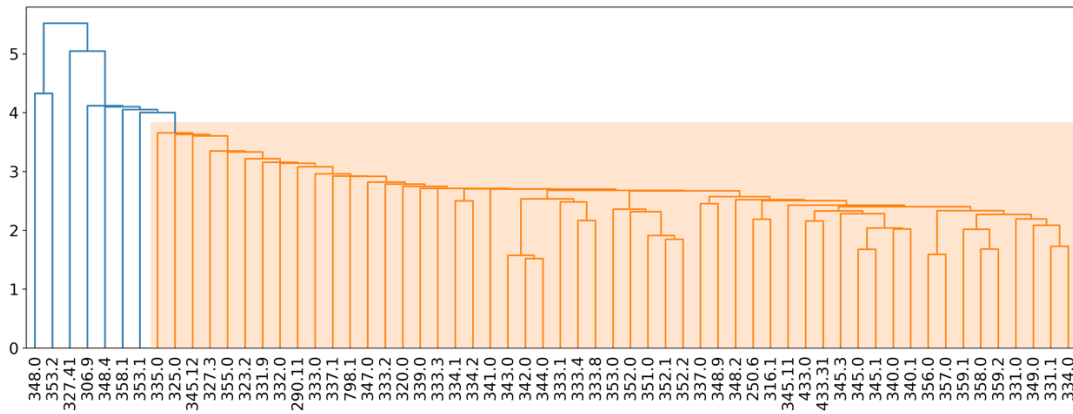


RESP



E

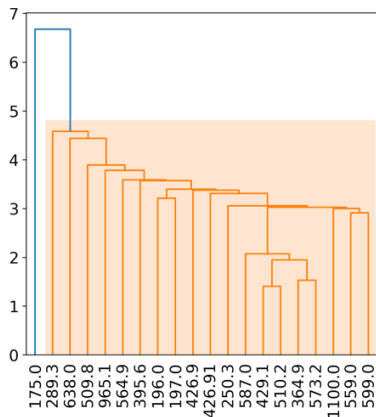
NEURO



F

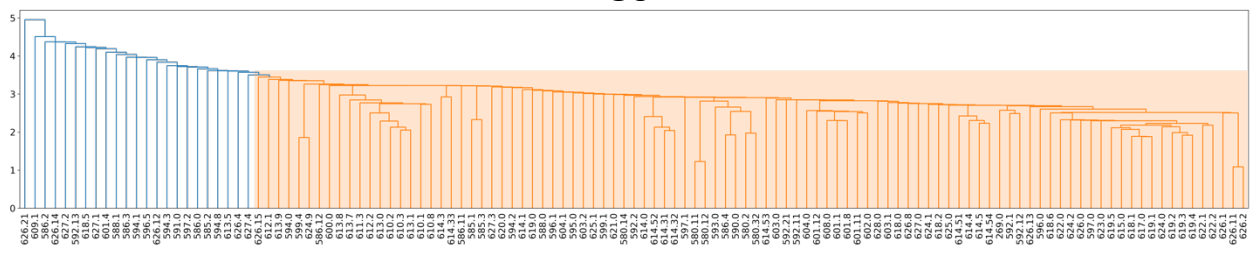
INF

G



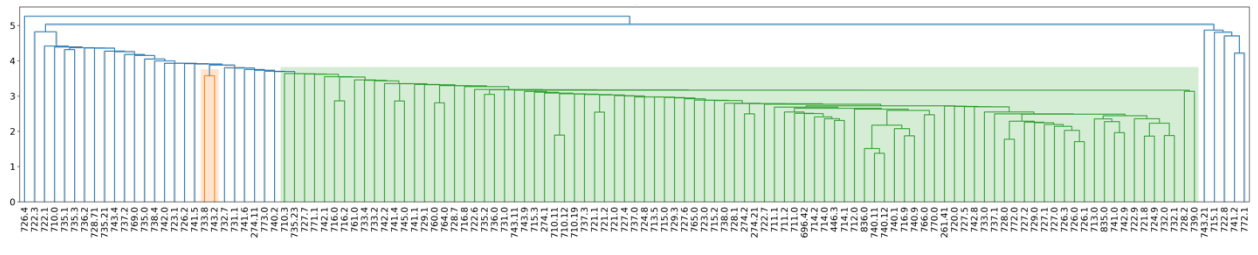
GU

H



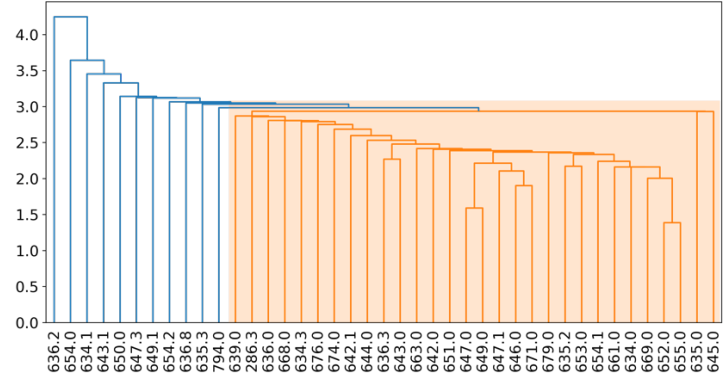
MSK

I



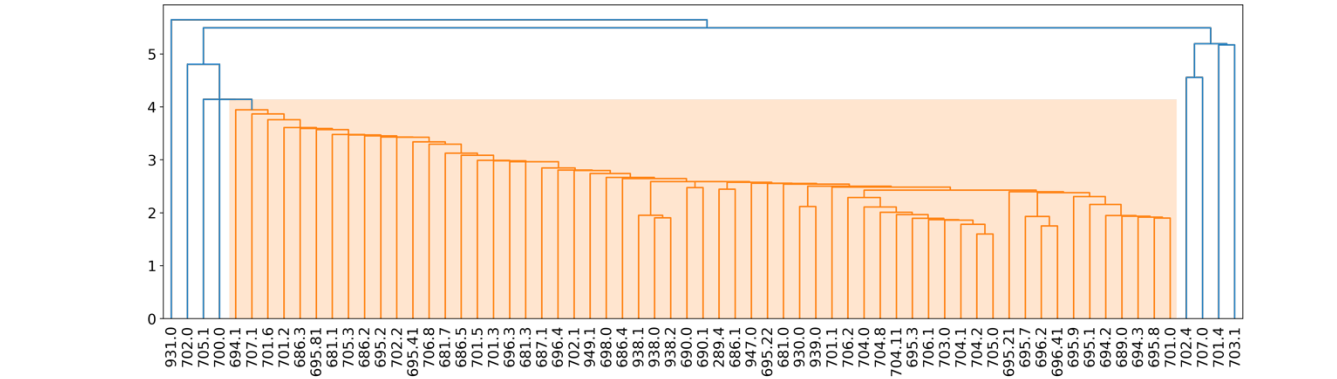
GYN

J

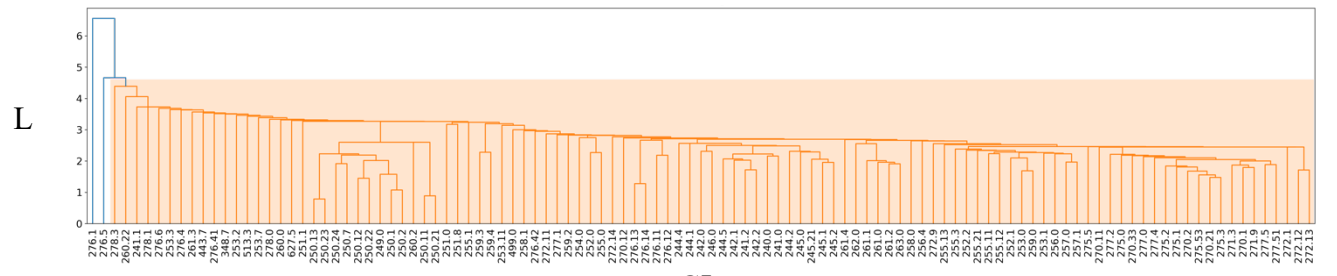


K

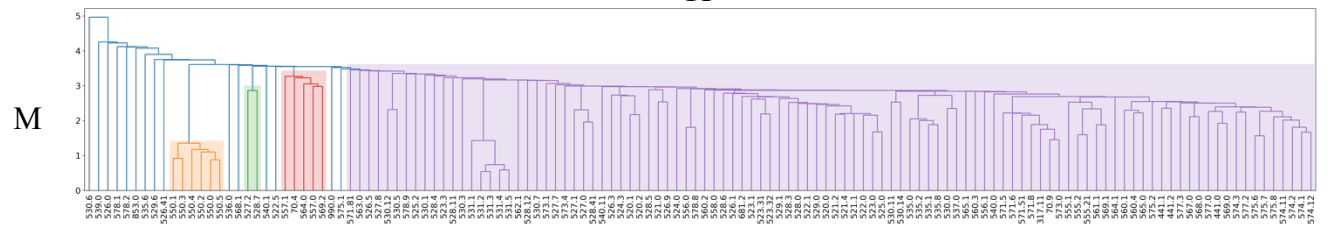
SKIN



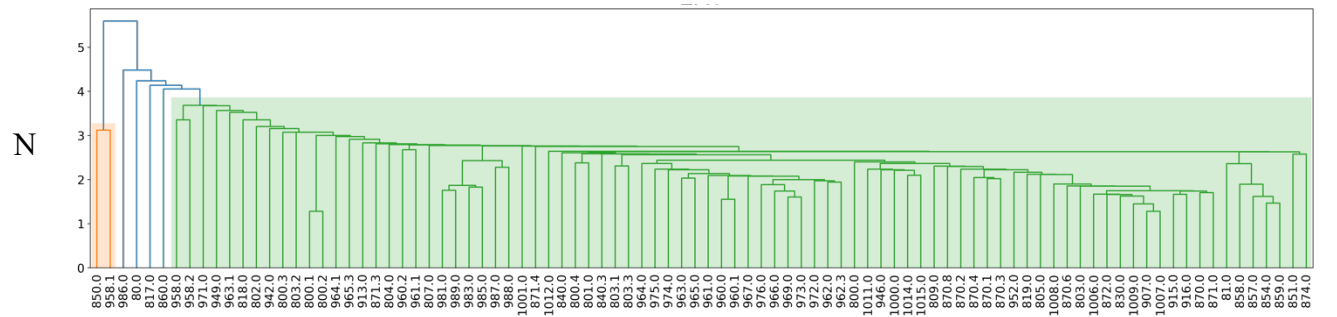
ENDO



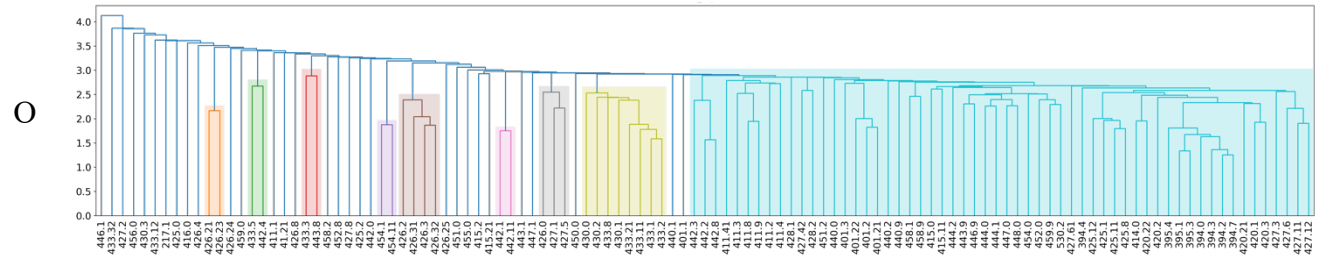
GI



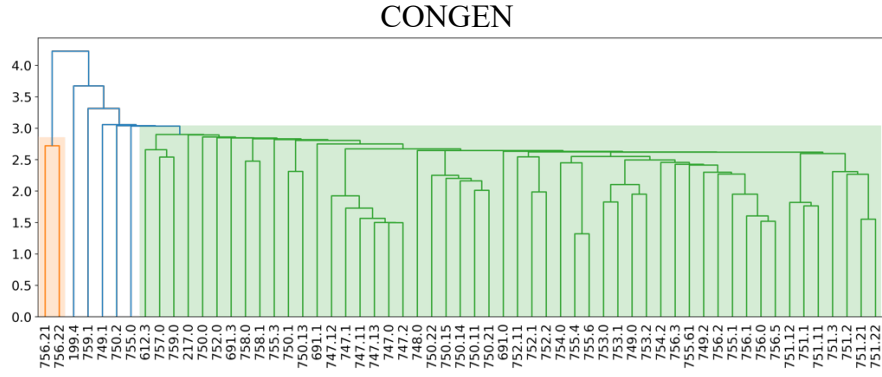
EXT



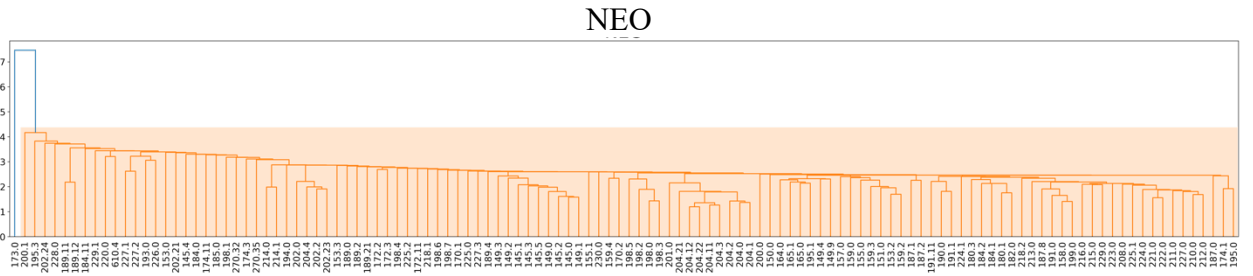
CV



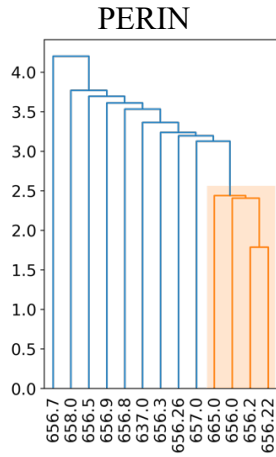
P



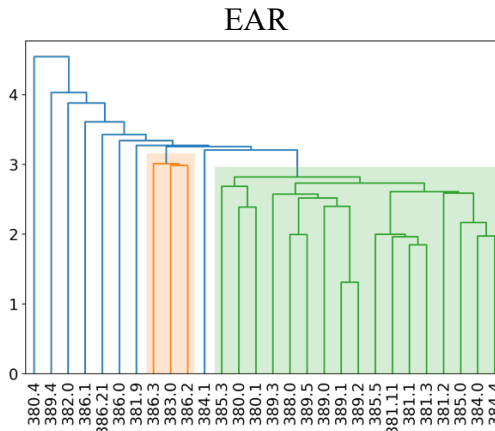
Q



R



S



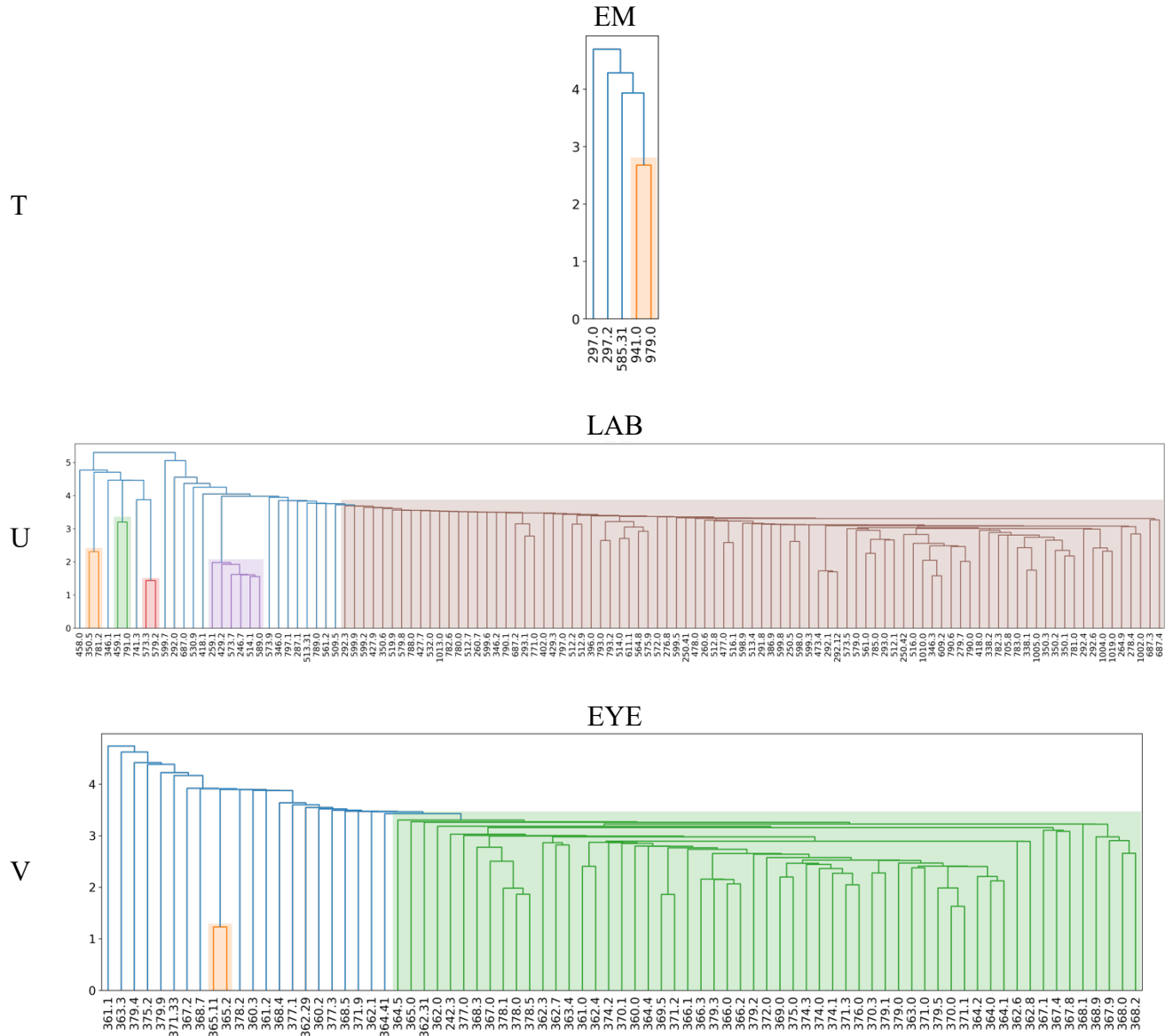


Figure S3. Dendrograms of phenotype representations in 22 disease categories. The Phecodes are clustered based on the embedding similarity from POPDx.

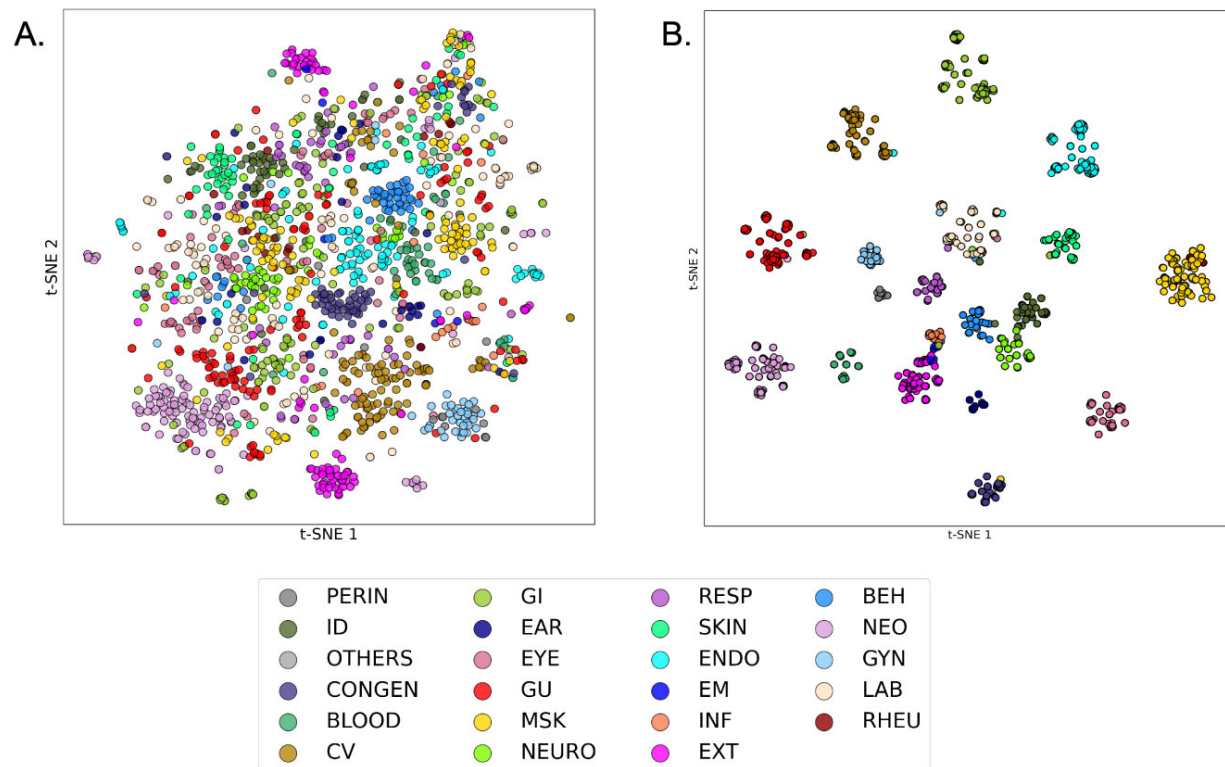


Figure S4. The structure-based embeddings and NLP-based embeddings of phenotypes. (A) The t -SNE plot shows less segregation of phenotypes using the semantic embedding method. (B) The t -SNE plot shows the segregation of phenotypes into different disease categories using the structure-based embedding method.

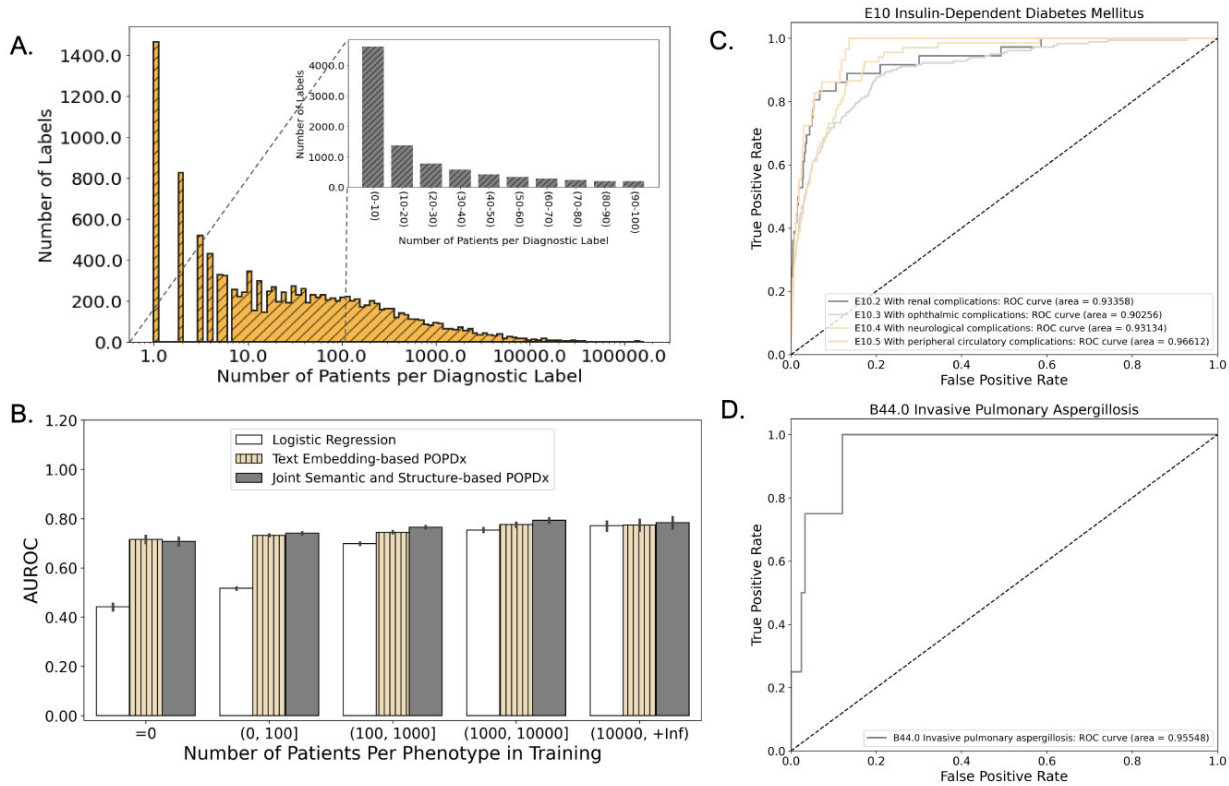


Figure S5. The POPDx performance for patient phenotyping of 12,803 ICD-10 codes in the UK Biobank study. (A) The long-tailed distributions of the ICD-10 diagnostic labels present a challenging dataset with heavy data imbalance. (B) A bar plot comparing POPDx with other models in terms of AUROC scores. (C) The ROC curves for phenotypes related to insulin-dependent diabetes mellitus (seen phenotypes in training). (D) The ROC curve of a rare phenotype in training.

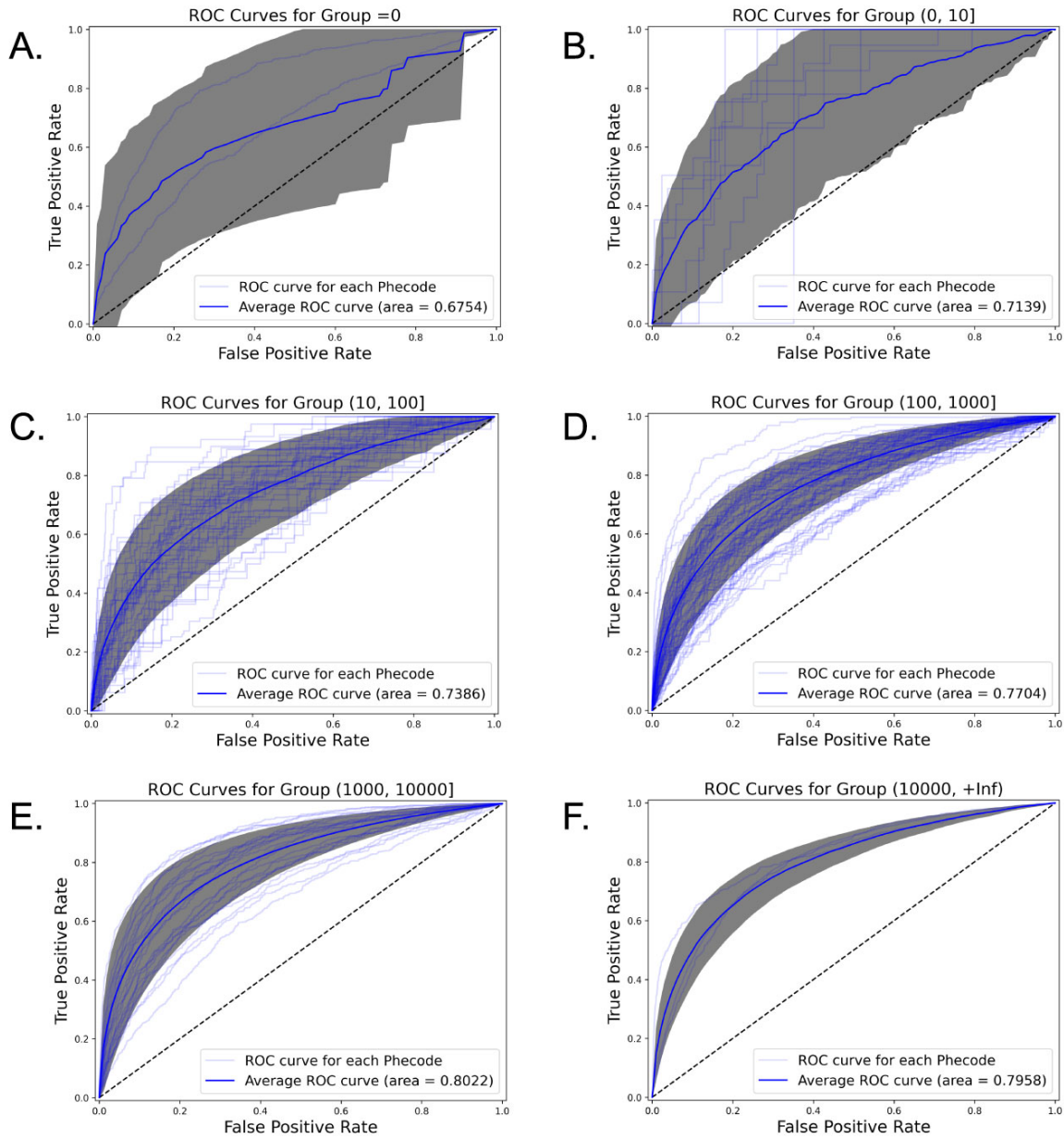


Figure S6. The POPDx performance on test sets for patient phenotyping of 1,538 Phecodes in the UK Biobank study. ROC curves across six groupings of Phecodes are represented respectively: (A) 0 samples (B) (0, 10] samples (C) (10, 100] samples (D) (100, 1000] samples (E) (1000, 10000] samples (F) (10000, +Inf) samples in the training set. A random selection of the ROC curves is shown to aid the eye.